Knee joint angle estimation by sequential correction of gyroscope bias

AYUKO SAITO (saito@cc.kogakuin.ac.jp)
Kogakuin Daigaku https://orcid.org/0000-0002-1675-8049
YUTAKA TANZAWA
Kogakuin University: Kogakuin Daigaku
SATORU KIZAWA
National Institute of Technology, Akita College

Research Article

Keywords: Bias error, Gyro sensor, Knee joint angle, Motion sensor, Sensor fusion

Posted Date: July 13th, 2021

DOI: https://doi.org/10.21203/rs.3.rs-697958/v1

RESEARCH

Knee joint angle estimation by sequential correction of gyroscope bias

Ayuko SAITO[1]*, Yutaka TANZAWA[1] and Satoru KIZAWA[2]

Corresponding author

Correspondence to Ayuko SAITO.

E-mail of corresponding author: saito@cc.kogakuin.ac.jp

Abstract

Compact and lightweight nine-axis motion sensors have come to be used for motion analysis in a variety of fields such as medical care, welfare, and sports. Nine-axis motion sensors include a three-axis gyroscope, a three-axis accelerometer, and a three-axis magnetometer and can estimate joint angles using the gyroscope outputs. However, the bias of the gyroscope is often unstable depending on the measurement environment and the accuracy of the gyroscope itself, causing error to accumulate in the angle obtained by integrating the gyroscope output. Although several sensor fusions have been proposed for pose estimation, such as using an accelerometer and a magnetometer, sequentially estimating and correcting the bias of the gyroscope are desirable for more accurate pose estimation. In addition, considering accelerations other than the acceleration due to gravity is important for a sensor fusion method that utilizes the accelerometer to correct the gyroscope output. Therefore, in this study, an extended Kalman filter algorithm was developed to sequentially correct both the gyroscope bias and the centrifugal and tangential acceleration of an accelerometer. The gait measurement results indicate that the proposed method successfully suppresses drift in the estimated knee joint angle over the entire measurement time of knee angle measurement during gait. The knee joint angles estimated using the proposed method were generally consistent with results obtained from an optical 3D motion analysis system. The proposed method is expected to be useful for estimating motion in medical care and welfare applications.

Keywords: Bias error, Gyro sensor, Knee joint angle, Motion sensor, Sensor fusion

Introduction

Nine-axis motion sensors used for motion analysis include a three-axis gyroscope to measure angular velocity, a three-axis accelerometer to measure acceleration, and a three-axis magnetometer

to measure the magnetic field. The sensor pose can be estimated sequentially by integrating the roll, pitch, and yaw rates [1] using the known initial pose and gyroscope output. However, the gyroscope has several sources of error, including a bias error, a scale factor error, a misalignment error, and noise [2]. The scale factor error is the deviation from the ideal sensitivity, and the misalignment error is the deviation from the ideal alignment of the axes. The scale factor and misalignment errors, which also arise from the accelerometer and magnetometer, can be corrected in advance using measurement data; this generally eliminates the need for users to correct these errors because most commercially available nine-axis motion sensors have been calibrated prior to shipment from the factory. In contrast, the bias, which is the output when the input angular velocity is 0, changes over time, meaning the bias of the gyroscope must be corrected before each measurement. Because the pose estimation accuracy decreases with the integration of bias errors, several pose estimation methods based on sensor fusion using an accelerometer and a magnetometer have been proposed [3, 4]. Therefore, compact and lightweight nine-axis motion sensors have come to be used for motion measurement in a wide range of fields such as medical care, welfare, and sports [5–7]. Kalman filtering [8–12] and complementary filtering [13–17] are some pose estimation methods using sensor fusion.

The Kalman filter, which does not require the accumulation of all of the time series data, estimates the current state recursively by using the state in the previous time step. The Kalman filter has the advantage of being able to estimate the system state with a small computational load. Several Kalman filters for pose estimation have been used to construct the state equation using the roll, pitch, and yaw rates. One observation equation proposed for use in such methods uses the yaw angle calculated from the magnetometer output and takes advantage of the fact that the accelerometer detects only the acceleration due to gravity when it is at rest [18]. Because the magnetic field cannot be measured correctly using a magnetometer in a variable magnetic field, several sensor fusion methods that can correct the magnetometer output under a variable magnetic field have been proposed [19, 20]. Moreover, sensor fusion approaches that consider accelerations other than the acceleration due to gravity have been proposed [21–23]. These sensor fusion methods contribute to the increased accuracy of the pose estimation. However, the bias of the gyroscope is often unstable depending on the measurement environment and the accuracy of the gyroscope itself. In the Kalman filter for pose estimation, the prediction based on the gyroscope output and the observation values, which include the accelerometer and magnetometer outputs, are used in a complementary manner. Therefore, increasing the accuracy of the pose estimation requires the sequential estimation and correction of the bias of the gyroscope.

For the estimation of the knee joint angle during walking in this study, a Kalman filter was devised to sequentially correct the bias error of the gyroscope and the output of the accelerometer based on existing reports [24, 25]. Previous studies have shown that the knee joint angle can be

estimated accurately by attaching motion sensors to the center of the anterior surface of the thigh and shank. Therefore, in this study, as a first step to apply the proposed method to human pose estimation, the knee joint angle during walking was focused on. Human locomotion is produced by the rotational motion of the respective joints, causing the proportion of the centrifugal acceleration and the tangential acceleration in a part of the body to increase during exercise. Thus, the proposed method considered the centrifugal and tangential acceleration to correct the accelerometer output. During a laboratory experiment, the knee joint angles of four participants were measured using an optical 3D motion analysis system and two nine-axis motion sensors while the participants were walking. The accuracy of the proposed method was verified by comparing the obtained results with those obtained by sensor fusion with the sequential correction of the bias error of the gyroscope and the output of the accelerometer and those obtained with an optical 3D motion analysis system.

Measurement method

The 3D posture of the nine-axis motion sensor is represented by the Euler angles: the roll angle φ about the x-axis, the pitch angle θ about the y-axis, and the yaw angle ψ about the z-axis. Figure 1 shows the definition of the knee joint angle and the reference coordinate system. The reference coordinate system is a right-handed system with a vertical z-axis. The counterclockwise direction is defined as the positive direction.

The two motion sensors were attached to the center of the anterior surface of the thigh and shank. The thigh was defined as link $i-1$, and the shank was defined as link i. The y-axis of the sensor was defined as being parallel to the length direction of the thigh and shank. The knee joint angle in the sagittal plane was defined as the angle between the y-axis of the sensor attached to the thigh and that of the sensor attached to the shank.

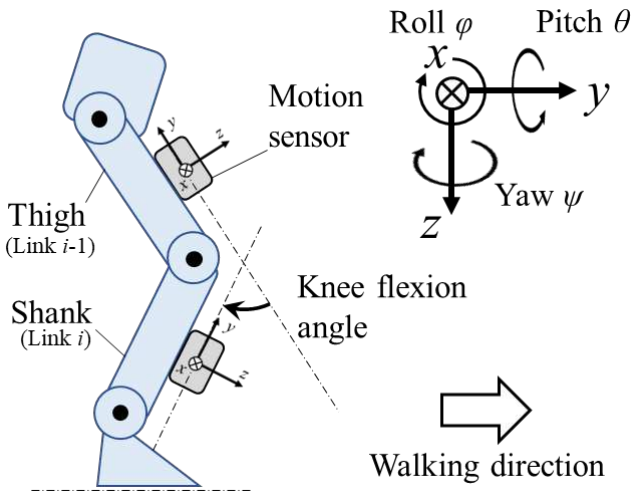

Fig. 1 Definitions of the knee joint angle and the reference coordinate system.

The following equations demonstrate how to calculate the initial roll and pitch angles using only the accelerometer outputs with the accelerometer at rest [4, 26]:

$$ {}^{i}\varphi_A = atan2\frac{{}^{i}A_y}{{}^{i}A_z} \qquad \left(-\pi < {}^{i}\varphi_A < \pi\right) \tag{1} $$

$$ {}^{i}\theta_A = atan2\frac{-{}^{i}A_x}{\sqrt{{}^{i}A_y{}^{2} + {}^{i}A_z{}^{2}}} \qquad \left(-\pi < {}^{i}\theta_A < \pi\right) \tag{2} $$

where the index i represents the ith link, which is the shank; ${}^{i}A_x$, ${}^{i}A_y$, and ${}^{i}A_z$ respectively denote the accelerometer output for the x-, y-, and z-axes; and ${}^{i}\varphi_A$ and ${}^{i}\theta_A$ respectively denote the initial roll and pitch.

The initial yaw is calculated from the magnetic field. However, the magnetic field cannot be measured accurately using a magnetometer in a variable magnetic field such as in a reinforced concrete structure [27–29]. Thus, the magnetic field in the laboratory was measured in advance to determine the appropriate sensitivity and offset parameters to correct the magnetometer output with the following relation:

$$ {}^{i}M = {}^{i}G\ {}^{i}m + {}^{i}B, \tag{3} $$

where

$$ {}^{i}M = \begin{bmatrix} {}^{i}M_x \\ {}^{i}M_y \\ {}^{i}M_z \end{bmatrix}, \quad {}^{i}m = \begin{bmatrix} {}^{i}m_x \\ {}^{i}m_y \\ {}^{i}m_z \end{bmatrix}, \quad {}^{i}G = \begin{bmatrix} {}^{i}G_x & 0 & 0 \\ 0 & {}^{i}G_y & 0 \\ 0 & 0 & {}^{i}G_z \end{bmatrix}, \quad {}^{i}B = \begin{bmatrix} {}^{i}B_x \\ {}^{i}B_y \\ {}^{i}B_z \end{bmatrix}. $$

Here, ${}^{i}M_x$, ${}^{i}M_y$, and ${}^{i}M_z$ respectively denote the x-, y-, and z-components of the magnetometer outputs; ${}^{i}m_x$, ${}^{i}m_y$, and ${}^{i}m_z$ respectively denote the x-, y-, and z-components of the corrected magnetic field data ; ${}^{i}G_x$, ${}^{i}G_y$, and ${}^{i}G_z$ respectively denote the sensitivity parameters for the x-, y-, and z-components; and ${}^{i}B_x$, ${}^{i}B_y$, and ${}^{i}B_z$ respectively denote the offset parameters in the x-, y-, and z-directions.

The incline of yaw angle is calculated from the roll ${}^{i}\varphi_A$, pitch ${}^{i}\theta_A$, and magnetometer output as

$$ \begin{bmatrix} {}^{c,i}m_x \\ {}^{c,i}m_y \\ {}^{c,i}m_z \end{bmatrix} = \begin{bmatrix} \cos{}^{i}\theta_A & \sin{}^{i}\varphi_A\sin{}^{i}\theta_A & \cos{}^{i}\varphi_A\sin{}^{i}\theta_A \\ 0 & \cos{}^{i}\varphi_A & -\sin{}^{i}\varphi_A \\ -\sin{}^{i}\theta_A & \sin{}^{i}\varphi_A\cos{}^{i}\theta_A & \cos{}^{i}\varphi_A\cos{}^{i}\theta_A \end{bmatrix} \begin{bmatrix} {}^{i}m_x \\ {}^{i}m_y \\ {}^{i}m_z \end{bmatrix}, \tag{4} $$

where ${}^{i}m_x$, ${}^{i}m_y$, and ${}^{i}m_z$ respectively denote the x-, y-, and z-components of the magnetic

field data after variable magnetic field correction and ${}^{c,i}m_x$, ${}^{c,i}m_y$, and ${}^{c,i}m_z$ respectively represent the *x*-, *y*-, and *z*-components of the magnetic field data after inclination correction.

From this, the following equation is used to calculate the initial yaw:

$$ {}^{i}\psi_m = atan2\frac{-{}^{c,i}m_y}{{}^{c,i}m_x} \qquad \left(-\pi < {}^{i}\psi_m < \pi\right). \tag{5}$$

The roll–pitch–yaw differentials in the absolute coordinate are given by

$$\begin{bmatrix} {}^{i}\dot{\psi} \\ {}^{i}\dot{\theta} \\ {}^{i}\dot{\varphi} \end{bmatrix} = \begin{bmatrix} 0 & \sin {}^{i}\varphi\sec {}^{i}\theta & cos\ {}^{i}\varphi\sec {}^{i}\theta \\ 0 & \cos {}^{i}\varphi & -\sin {}^{i}\varphi \\ 1 & \sin {}^{i}\varphi\tan {}^{i}\theta & \cos {}^{i}\varphi\tan {}^{i}\theta \end{bmatrix} \begin{bmatrix} {}^{i}\omega_x \\ {}^{i}\omega_y \\ {}^{i}\omega_z \end{bmatrix}, \tag{6}$$

where ${}^{i}\dot{\varphi}$, ${}^{i}\dot{\theta}$, and ${}^{i}\dot{\psi}$ respectively denote the differentials of the roll, pitch, and yaw, and ${}^{i}\omega_x$, ${}^{i}\omega_y$, and ${}^{i}\omega_z$ respectively denote the *x*-, *y*-, and *z*-components of the gyroscope outputs. From this, the roll, pitch, and yaw angles are calculated by substituting Eq. (6) into the following equation:

$$\begin{bmatrix} {}^{i}\psi \\ {}^{i}\theta \\ {}^{i}\varphi \end{bmatrix}_{t+1} = \int \begin{bmatrix} {}^{i}\dot{\psi} \\ {}^{i}\dot{\theta} \\ {}^{i}\dot{\varphi} \end{bmatrix} \mathrm{d}t + \begin{bmatrix} {}^{i}\psi \\ {}^{i}\theta \\ {}^{i}\varphi \end{bmatrix}_{t}, \tag{7}$$

where t and $t + 1$ denote sequential time steps.

Eqs. (1)–(7) are also available for the link $i - 1$, which represents the thigh.

Extended Kalman filter

A state-space model consisting of the nonlinear state equation and the nonlinear observation equation was constructed to estimate the knee joint angle.

Nonlinear state equation

The gyro bias dynamics are expressed empirically as [2, 30]

$$\begin{bmatrix} \dot{b}_{x,t} \\ \dot{b}_{y,t} \\ \dot{b}_{z,t} \end{bmatrix} = \begin{bmatrix} -\beta_x & 0 & 0 \\ 0 & -\beta_y & 0 \\ 0 & 0 & -\beta_z \end{bmatrix} \begin{bmatrix} b_{x,t} \\ b_{y,t} \\ b_{z,t} \end{bmatrix} + w_t, \tag{8}$$

where $\dot{b}_{x,t}$, $\dot{b}_{y,t}$, and $\dot{b}_{z,t}$ respectively denote the *x*-, *y*-, and *z*-components of the bias rates; $b_{x,t}$,

$b_{y,t}$, and $b_{z,t}$ respectively denote the *x*-, *y*-, and *z*-components of the bias of the gyroscope; β_x, β_y, and β_z are parameters set to $\beta_x = \beta_y = \beta_z = 0.00001$ in this study; and w_t is white noise.

The bias of the gyroscope is estimated as a state value using Eq. (8). Furthermore, the estimated bias is removed from the gyroscope output by applying Eq. (7) to the following nonlinear state equation:

$$ {}^{i}x_{t+1} = {}^{i}F({}^{i}x_t) + {}^{i}w_t, \tag{9}$$

where

$$ {}^{i}x_t = \begin{bmatrix} {}^{i}\psi_t \\ {}^{i}\theta_t \\ {}^{i}\varphi_t \\ {}^{i}b_{x,t} \\ {}^{i}b_{y,t} \\ {}^{i}b_{z,t} \end{bmatrix}, $$

$$ {}^{i}F({}^{i}x_t) $$

$$ = \begin{bmatrix} {}^{i}\psi_t + sin\ {}^{i}\varphi_t sec\ {}^{i}\theta_t \cdot \left({}^{i}\omega_{y,t} - {}^{i}b_{y,t} \right) \cdot Ts + cos\ {}^{i}\varphi_t sec\ {}^{i}\theta_t \cdot \left({}^{i}\omega_{z,t} - {}^{i}b_{z,t} \right) \cdot Ts \\ {}^{i}\theta_t + cos\ {}^{i}\varphi_t \cdot \left({}^{i}\omega_{y,t} - {}^{i}b_{y,t} \right) \cdot Ts - sin\ {}^{i}\varphi_t \cdot \left({}^{i}\omega_{z,t} - {}^{i}b_{z,t} \right) \cdot Ts \\ {}^{i}\varphi_t + \left({}^{i}\omega_{x,t} - {}^{i}b_{x,t} \right) \cdot Ts + sin\ {}^{i}\varphi_t tan\ {}^{i}\theta_t \cdot \left({}^{i}\omega_{y,t} - {}^{i}b_{y,t} \right) \cdot Ts + cos\ {}^{i}\varphi_t tan\ {}^{i}\theta_t \cdot \left({}^{i}\omega_{z,t} - {}^{i}b_{z,t} \right) \cdot Ts \\ {}^{i}b_{x,t} - \beta_x \cdot {}^{i}b_{x,t} \cdot Ts \\ {}^{i}b_{y,t} - \beta_y \cdot {}^{i}b_{y,t} \cdot Ts \\ {}^{i}b_{z,t} - \beta_z \cdot {}^{i}b_{z,t} \cdot Ts \end{bmatrix} $$

$$ {}^{i}w_t = \begin{bmatrix} 0 \\ 0 \\ 0 \\ {}^{i}w_{x,t} \\ {}^{i}w_{y,t} \\ {}^{i}w_{z,t} \end{bmatrix}. $$

Furthermore, the index *i* represents link *i*, which is defined as the shank, and *Ts* is the sampling time. Lines 1–3 of the state equation are constructed from Eq. (7), where the estimated bias errors ${}^{i}b_{x,t}$, ${}^{i}b_{y,t}$, and ${}^{i}b_{z,t}$ are removed from the gyroscope output ${}^{i}\omega_{x,t}$, ${}^{i}\omega_{y,t}$, and ${}^{i}\omega_{z,t}$. Lines 4–6 of the state equation is constructed from Eq. (8).

Eq. (9) can also be applied to link $i - 1$, which represents the thigh.

Nonlinear state equation

The accelerometer output A_s includes the translational acceleration A_{tr}, the centrifugal and tangential accelerations A_{ct}, and the gravitational acceleration g, as described by

$$A_s = A_{tr} + A_{ct} + g. \tag{10}$$

The centrifugal and tangential accelerations are given by the gyroscope output. Therefore, the sums of the centrifugal and tangential accelerations in the thigh and shank are respectively given by

$$^{i-1}A_{ct} = {}^{i-1}\omega \times {}^{i-1}\omega \times {}^{i-1}r + {}^{i-1}\dot{\omega} \times {}^{i-1}r \tag{11}$$

$$^{i}A_{ct} = {}^{i}\omega \times {}^{i}\omega \times {}^{i}r + {}^{i}\dot{\omega} \times {}^{i}r, \tag{12}$$

where $i-1$ and i respectively denote the links representing the thigh and shank and $^{i-1}\omega$ and $^{i}\omega$ respectively denote the gyroscope outputs in the thigh and shank. In addition, ^{i-1}r is the distance from the anterior surface of the great trochanter to the sensor attached to the thigh, and ^{i}r is the distance from the height of the lateral condyle of the tibia to the sensor attached to the shank. The positions of the great trochanter and the lateral condyle of the tibia were determined by referring to the existing literature [31]. The differentials of the gyroscope outputs are denoted $^{i-1}\dot{\omega}$ and $^{i}\dot{\omega}$. The gyroscope outputs are differentiated with the following equation:

$$D(s) = \frac{s}{1+ns}, \tag{13}$$

where $D(s)$ is the inexact differential, s is the Laplace operator, and n is the time constant. In this study, the time constant was set to $n = 0.01$.

The nonlinear observation equation in the thigh was constructed using Eqs. (5), (10), and (11) as follows:

$$^{i-1}y_t = {}^{i-1}H(x_t) + {}^{i-1}v_t, \tag{14}$$

where

$$^{i-1}y_t = \begin{bmatrix} {}^{i-1}\psi_{m,t} \\ {}^{i-1}A_{s_x,t} - {}^{i-1}A_{ct_x,t} \\ {}^{i-1}A_{s_y,t} - {}^{i-1}A_{ct_y,t} \\ {}^{i-1}A_{s_z,t} - {}^{i-1}A_{ct_z,t} \end{bmatrix}, \quad {}^{i-1}H(x_t) = \begin{bmatrix} {}^{i-1}\psi_t \\ ({}^{o}R_{i-1})_t^T \begin{bmatrix} 0 \\ 0 \\ g \end{bmatrix} \end{bmatrix}.$$

Here, ${}^{i-1}\psi_{m,t}$ denotes the yaw angle given in Eq. (5) as ${}^{i-1}\psi_t$; ${}^{i-1}A_{s_x,t}$, ${}^{i-1}A_{s_y,t}$, and ${}^{i-1}A_{s_z,t}$ respectively denote the *x*-, *y*-, and *z*-components of the accelerometer outputs; ${}^{i-1}A_{ct_x,t}$, ${}^{i-1}A_{ct_y,t}$, and ${}^{i-1}A_{ct_z,t}$ respectively denote the *x*-, *y*-, and *z*-components of the sums of the centrifugal and tangential accelerations of the thigh; $({}^{o}R_{i-1})_t$ denotes the rotational matrix from the reference coordinate system to the $i-1$ sensor coordinate system; and ${}^{i-1}v_t$ is white noise.

The translational acceleration of the thigh, which is expressed as the sum of the centrifugal and tangential accelerations of the lumbar, was not considered because the lumbar showed negligible motion in comparison with thigh. Therefore, the nonlinear observation equation for the thigh contains only the centrifugal, tangential, and gravitational accelerations.

The nonlinear observation equation in the shank was constructed using Eqs. (5), (10), (11), and (12) as follows:

$$ {}^{i}y_t = {}^{i}H(x_t) + {}^{i}v_t, \tag{15}$$

where

$${}^{i}y_t = \begin{bmatrix} {}^{i}\psi_{m,t} \\ {}^{i}A_{s_x,t} - {}^{i}A_{ct_x,t} \\ {}^{i}A_{s_y,t} - {}^{i}A_{ct_y,t} \\ {}^{i}A_{s_z,t} - {}^{i}A_{ct_z,t} \end{bmatrix},$$

$${}^{i}H(x_t) = \begin{bmatrix} {}^{i}\psi_t \\ ({}^{o}R_i)_t^T \begin{bmatrix} 0 \\ 0 \\ g \end{bmatrix} + ({}^{o}R_i)_t^T \cdot ({}^{o}R_{i-1})_t \cdot \left({}^{i-1}\omega \times {}^{i-1}\omega \times {}^{i-1}r + {}^{i-1}\dot{\omega} \times {}^{i-1}r\right) \end{bmatrix}.$$

Here, the variables are defined in the same manner as in Eq. (14) but for the shank. The translational acceleration of the shank is expressed as the sum of the centrifugal and tangential accelerations of the thigh [23].

Extended Kalman filter algorithm

The partial derivatives of $F(x_t)$ and $H(x_t)$ are given by

$$f(x_t) = \frac{\partial F(x_t)}{\partial x_t} \tag{16}$$

$$h(x_t) = \frac{\partial H(x_t)}{\partial x_t}. \tag{17}$$

Then, the prediction (Eqs. (18) and (19)) and filtering (Eqs. (20)–(22)) are performed using the nonlinear discrete-time system represented by Eqs. (9), (14), and (15) as

$$x_{t+1}^{-} = F(x_t) \tag{18}$$

$$P_{t+1}^{-} = f_t P_t f_t^T + Q \tag{19}$$

$$K_{t+1} = P_{t+1}^{-} h_{t+1}^T (h_{t+1} P_{t+1}^{-} h_{t+1}^T + R)^{-1} \tag{20}$$

$$x_{t+1} = x_{t+1}^{-} + K_{t+1}\left(y_{t+1} - H(x_{t+1}^{-})\right) \tag{21}$$

$$P_{t+1} = (I - K_{t+1} h_{t+1}) P_{t+1}^{-}, \tag{22}$$

where P is the error covariance matrix, K is the Kalman gain, and Q and R respectively represent the covariance matrices of the white noise w_t and v_t.

The roll–pitch–yaw angles of each segment obtained from the sensor fusion are converted into a rotational matrix in the absolute coordinate system as

$$({}^{o}R_i)_t = \begin{bmatrix} \cos {}^{i}\psi_t & -\sin {}^{i}\psi_t & 0 \\ \sin {}^{i}\psi_t & \cos {}^{i}\psi_t & 0 \\ 0 & 0 & 1 \end{bmatrix} \cdot \begin{bmatrix} \cos {}^{i}\theta_t & 0 & \sin {}^{i}\theta_t \\ 0 & 1 & 0 \\ -\sin {}^{i}\theta_t & 0 & \cos {}^{i}\theta_t \end{bmatrix} \cdot \begin{bmatrix} 1 & 0 & 0 \\ 0 & \cos {}^{i}\varphi_t & -\sin {}^{i}\varphi_t \\ 0 & \sin {}^{i}\varphi_t & \cos {}^{i}\varphi_t \end{bmatrix}. \tag{23}$$

The rotational matrix from the i coordinate system to the $i-1$ coordinate system is then calculated by substituting Eq. (23) into the following equation:

$$\left({}^{i-1}R_i\right)_t = ({}^{o}R_{i-1})_t^T \cdot ({}^{o}R_i)_t. \tag{24}$$

Experiment

The walking gaits of four healthy adults (participants A, B, C, and D) were experimentally measured. The anthropometric data are given in Table 1. After the purpose and requirements of the study were explained, the participants gave written informed consent to participation. Study approval was obtained from the Research Ethics Board of Kogakuin University and the National Institute of Technology, Akita College.

During the experiment, an optical 3D motion analysis system (Bonita 10, Vicon Motion Systems, Ltd., or MAC3D, Motion Analysis Ltd.) and two nine-axis motion sensors (SS-WS1792, Sports Sensing Co., Ltd.) were used to measure the gait of the participants. The positions of the

Table 1 Anthropometric data.

Participant	Height [m]	Weight [kg]	Age (years)
A	1.76	58	19
B	1.80	56	19
C	1.81	64	19
D	1.68	80	21

reflective markers for the optical 3D motion analysis system were found by referring to the Vicon Plug-in Gait model. The nine-axis motion sensor used for this study includes a three-axis gyroscope (±1500 dps), a three-axis accelerometer (±16 G), and a three-axis magnetometer (±10 Gauss). This sensor measures 38 mm × 53 mm × 11 mm and weighs 30 g. Motion sensors were attached to the right thigh and shank of the participants. The heel strike was defined as the time when the z-coordinate of the reflective marker attached to the right heel was at a minimum. The sampling frequencies of the nine-axis motion sensors and the optical 3D motion analysis system were 100 Hz.

Measurement was initiated in each trial when the participant was upright and stationary. After maintaining an upright posture for approximately 3 s, the participant took their first step with the left foot. They were instructed to walk using a natural stride in time with a metronome (90 bpm). Measurement ended when the participant reached the goal tape that was 2.5 m from the start point, which was attached to the floor prior to the experiment.

Results and Discussion

Results over the entire measurement time

The knee joint angles of the four participants are shown in Fig. 2 over the entire measurement time for a single trial. The red curves represent the results obtained from the sensor fusion with no gyroscope correction, where Eq. (7) was applied to the nonlinear state equation given by Eq. (9) without estimating and removing the bias error of the gyroscope, correcting only the accelerometer outputs using Eqs. (14) and (15). The blue curves represent the results obtained from the proposed method, where the bias of the gyroscope was corrected using Eq. (9), in addition to the correction of the accelerometer outputs using Eqs. (14) and (15). Fig. 2(a)–(d) shows the results of single trials with large errors due to the bias of the gyroscope outputs.

The estimated knee angles obtained using the proposed method were almost 0° at the beginning and end of the measurement. In contrast, the results obtained from the sensor fusion without gyroscope bias correction gradually drifted from the beginning of the measurement and had positive and negative values after walking.

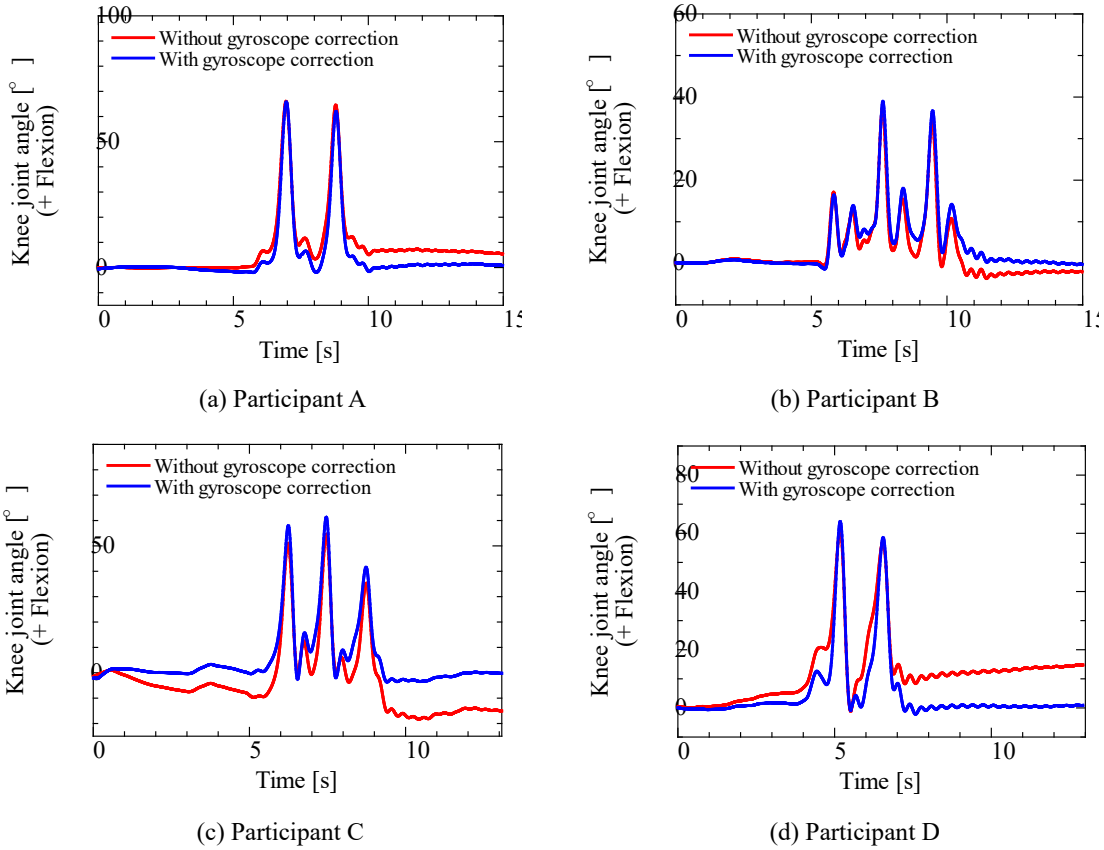

Fig. 2 Knee joint angles over the entire measurement time obtained from the two sensor fusion methods. The red curves represent the results obtained from the method with only accelerometer output correction. The blue curves represent the results obtained from the proposed method with both accelerometer and gyroscope output correction.

The estimated knee angles of participants C and D obtained without gyroscope correction showed large drift, indicating that the gyroscope outputs in these cases might have contained larger and more unstable biases or noise than those for the other two participants. However, because there was almost no drift in the knee angles of all participants using the proposed method, the results demonstrated that the proposed method is able to successfully remove the gyroscope bias and prevent drifting in the estimated angle.

Results during one gait cycle

The knee joint angles during one gait cycle for the four participants are shown in Fig. 3. The black curves show the measurement results obtained from the optical 3D motion analysis system. The solid red and blue curves are the same as in Fig. 2, i.e. the sensor fusion results without and with gyroscope bias correction, respectively. Fig. 3(a)–(d) corresponds to single gait cycles included in

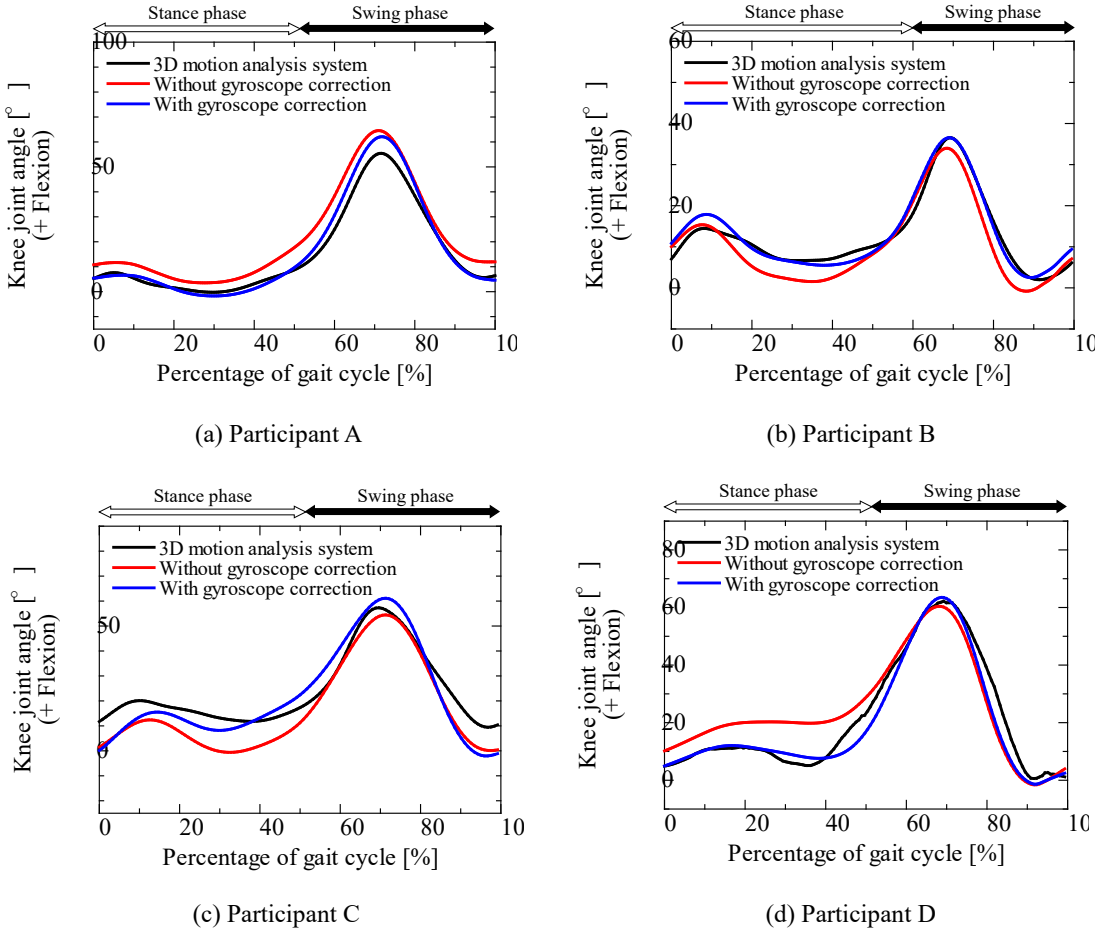

Fig. 3 Knee joint angles during one gait cycle obtained from the 3D motion analysis system and the two sensor fusion methods. The solid black curves show the results obtained from the 3D motion analysis system. The solid red curves show the results obtained from the method with only accelerometer output correction. The solid blue curves show the results obtained from the sensor fusion with both accelerometer and gyroscope output correction.

Table 2 Root mean square error of estimated knee angles.

Participant	RMSE [°]	
	Without gyroscope correction	With gyroscope correction
A	7.17	3.32
B	3.78	1.98
C	8.23	6.71
D	7.53	4.05

Fig. 2(a)–(d), respectively. The horizontal axis represents the normalized time, where one gait cycle is 100%. Table 2 gives the root mean square error (RMSE) between the knee joint angles estimated with the two sensor fusion methods and the angles obtained from the 3D motion analysis system.

The knee joint angles obtained from the proposed method are generally consistent with the results obtained using the optical 3D motion analysis system and showed the peak of the flexion in the midpoint of the stance phase and the last half of the swing phase. The results indicate that the knee joint angles were measured appropriately because those characteristics are similar to typical joint angle patterns that are recorded during walking [32].

The knee joint angle obtained from the method without gyroscope correction for participant A shows an upward offset against the result with gyroscope correction and that for participant B shows a downward offset against the result with gyroscope correction. In contrast, the knee joint angle obtained from the method without gyroscope correction for participants C and D show upward and downward offsets during one gait cycle against the results with gyroscope correction. The results indicate that the bias of the gyroscope might have been often unstable during the experiment.

The knee joint angles obtained from the proposed method had RMSEs below those of the method without gyroscope bias correction for every participant. Although the measurement results obtained using the proposed method for participants C and D have large RMSEs, Table 2 demonstrates that the error of the proposed method is still lower than that for the method without gyroscope correction. These results demonstrate the effectiveness of the proposed method.

Conclusions

In this study, a method of sequentially estimating and correcting the bias of gyroscope measurements of human gait was developed. The method also includes correction of the accelerometer output by considering the centrifugal and tangential accelerations in the output of the accelerometer. The knee joint angles of four healthy participants during a walking task were estimated using the proposed method. The results yielded the following conclusions.

1.

The proposed method prevented the drifting of the estimated angles over the entire measurement time, whereas the angles obtained by sensor fusion only accelerometer output correction drifted.

2.

The proposed method can contribute to the increased accuracy of knee joint angle estimation.

Improving the accuracy of motion measurement using a simple, compact, and lightweight motion

sensor is necessary for motion measurement in a wide range of fields. Screening for abnormal gait by detecting the difference in the range of motion of each joint during individual gait cycles is a promising technique in the medical and welfare fields. The proposed method is expected to be useful for various motion analysis applications.

Competing interests

The authors declare that they have no competing interests.

Funding

This work was supported by JSPS KAKENHI Grant Number JP 20K19588.

Authors' Contributions

Ayuko SAITO conceived the study and drafted the manuscript. Ayuko SAITO carried out all experiments. Ayuko SAITO and Yutaka TANZAWA analyzed the data. Satoru KIZAWA participated in the research design and sequence alignment. All authors read and approved the final manuscript.

Acknowledgments

Not applicable

Author details

Affiliations

Department of Mechanical Science and Engineering, Kogakuin University

2665-1 Nakanomachi, Hachioji, Tokyo 192-0015, Japan

Ayuko SAITO and Yutaka TANZAWA

Department of Mechanical Engineering and Robotics, National Institute of Technology (KOSEN), Akita College, 1-1 Iijima-Bunkyo-cho, Akita 011-8511, Japan

Satoru KIZAWA

References

1. Hasegawa, R., General method deriving kinematic equations for rotation representations, Transactions of the Society of Instrument and Control Engineers, Vol.40, No.11 (2004), pp.1160-1162, DOI: 10.9746/sicetr1965.40.1160 (in Japanese).
2. Suzuki, S., Tawara, M., Nakazawa, D. and Nonami, K., Research on attitude estimation algorithm under dynamic acceleration, Journal of the Robotics Society of Japan, Vol.26, No.6 (208), pp.626-634, DOI: 10.7210/jrsj.26.626 (in Japanese).

3. Sabatini, A. M., Quaternion-based extended Kalman filter for determining orientation by inertial and magnetic sensing, IEEE Transactions on Biomedical Engineering, Vol. 53, No. 7 (2006), pp.1346-1356, DOI: 10.1109/TBME.2006.875664.
4. Jurman, D., Jankovec, M., Kamnik, R. and Topic, M., Calibration and data fusion solution for the miniature attitude and heading reference system, Sensors and Actuators A: Physical, Vol.138, No.2 (2007), pp. 411-420, DOI: 10.1016/j.sna.2007.05.008.
5. King, K., Yoon, S. W., Perkins, N. C. and Najafi, K., Wireless MEMS inertial sensor system for golf swing dynamics, Sensors and Actuators, A: Physical, Vol.141, No.2 (2008), pp.619–630, DOI: 10.1016/j.sna.2007.08.028.
6. Pan, M. S., Huang, K. C., Lu, T. H. and Lin, Z. Y., Using accelerometer for counting and identifying swimming strokes, Pervasive and Mobile Computing, Vol.31 (2016), pp.37–49, DOI: 10.1016/j.pmcj.2016.01.011.
7. Nüesch, C., Roos, E., Pagenstert, G. and Mündermann, A., Measuring joint kinematics of treadmill walking and running: Comparison between an inertial sensor based system and a camera-based system, Journal of Biomechanics, Vol.57(2017), pp.32–38, DOI: 10.1016/j.jbiomech.2017.03.015.
8. Rigatos, G. G., Extended Kalman and Particle Filtering for sensor fusion in motion control of mobile robots, Mathematics and Computers in Simulation, Vol.81, No. 3 (2010), pp.590–607, DOI: 10.1016/j.matcom.2010.05.003.
9. Adachi, S. and Maruta, I., Fundamentals of Kalman filter (2012), pp. 95–111, Tokyo Denki University Press (in Japanese).
10. Ran, C. and Deng, Z., Self-tuning weighted measurement fusion Kalman filtering algorithm, Computational Statistics & Data Analysis, Vol.56, No. 6 (2012), pp.2112–2128, DOI: 10.1016/j.csda.2012.01.001.
11. Kamil, M., Chobtrong, T., Günes, E. and Haid, M., Low-cost object tracking with MEMS sensors, Kalman filtering and simplified two-filter-smoothing, Applied Mathematics and Computation, Vol.235 (2014), pp.323–331, DOI: 10.1016/j.amc.2014.03.015.
12. Zheng, Z., Qiu, H., Wang, Z., Luo, S. and Lei, Y., Data fusion based multi-rate Kalman filtering with unknown input for on-line estimation of dynamic displacements, Measurement, Vol.131 (2019), pp.211–218, DOI: 10.1016/j.measurement.2018.08.057.
13. Baerveldt, A. J. and Klang, R., A low-cost and low-weight attitude estimation system for an autonomous helicopter, Proceedings of IEEE International Conference on Intelligent Engineering Systems (1997), pp.391–395, DOI: 10. 10.1109/INES.1997.632450.
14. Mahony, R., Hamel, T. and Pflimlin, J. M., Complementary filter design on the special orthogonal group SO(3), Proceedings of the 44th IEEE Conference on Decision and Control, and the European Control Conference 2005 (2005), pp.1477–1484, DOI: 10.1109/CDC.2005.1582367.

15. Euston, M., Coote, P., Mahony, R., Kim, J. and Hamel, T., A complementary filter for attitude estimation of a fixed-wing UAV, Proceedings of 2008 IEEE/RSJ International Conference of Intelligent Robots and Systems (2008), pp.340–345, DOI: 10.1109/IROS.2008.4650766.
16. Mahony, R., Hamel, T. and Pflimlin, J. M., Nonlinear complementary filters on the special orthogonal group, IEEE Transactions on Automatic Control, Vol.53, No. 5 (2008), pp.1203–1218, DOI: 10.1109/TAC.2008.923738.
17. Sugihara, T., Masuya, K. and Yamamoto, M., A complementary filter for high-fidelity attitude estimation based on decoupled linear/nonlinear properties of inertial sensors, Journal of the Robotics Society of Japan, Vol.31, No.3 (2013), pp.251-262, DOI: 10.7210/jrsj.31.251 (in Japanese).
18. Saito, A., Kizawa, S., Kobayashi, Y. and Miyawaki, K., Pose estimation by extended Kalman filter using noise covariance matrices based on sensor output, ROBOMECH Journal, Vol.7, No.36 (2020), DOI: 10.1186/s40648-020-00185-y.
19. Kondo, A., Doki, H. and Hirose, K., A Study on calibration method of magnetic field sensor for body motion measurement using inertial sensor, Proceedings of the Sports Engineering and Human Dynamics (2013), DOI: 10.1299/jsmeshd.2013._212-1_. (in Japanese).
20. Saito, A., Nara, Y. and Miyawaki, K., A study on estimating knee joint angle using motion sensors under conditions of magnetic field variation, Transactions of the JSME(in Japanese), Vol.85, No.873 (2019), DOI: 10.1299/transjsme.19-00061.
21. Suh, Y. S., Park, S. K., Kang, H. J. and Ro, Y. S., Attitude estimation adaptively compensating external acceleration, JSME International Journal Series C Mechanical Systems, Machine Elements and Manufacturing, Vol.49, No. 1 (2006), pp.172-179, DOI: 10.1299/jsmec.49.172.
22. Hirose, K., Doki, H. and Kondo, A., Studies on orientation measurement in sports using inertial and magnetic field sensors, Japan Society of Sports Industry, Vol.22, No.2 (2012), pp.255-262, DOI: 10.5997/sposun.22.255 (in Japanese).
23. Saito, A., Miyawaki, K., Kizawa, S. and Kobayashi, Y., A study on estimating the knee joint angle during walking using the motion sensors (Focusing on the effect of centrifugal acceleration and tangential acceleration), Transactions of the JSME (in Japanese), Vol.84, No.857 (2018), DOI: 10.1299/transjsme.17-00488.
24. Tawara, M., Suzuki, S. and Nonami, K., Development of the attitude sensor with small scale, light weight, versatility, Transactions of the JSME(in Japanese), Vol.77, No.781 (2011), pp.3386-3397, DOI: 10.1299/kikaic.77.3386.
25. Ishiguro, H. and Saeki, M., Estimation of story deformation angle using a MEMS acceleration & gyro sensor, Proceedings of JSCE, Vol.74, No.2 (2018), pp. 571-578, DOI: 10.2208/jscejam.74.I_571 (in Japanese).
26. Vaganay, J., Aldon, M. J. and Fournier, A., Mobile robot attitude estimation by fusion of inertial

data, Proceedings of the IEEE International Conference on Robotics and Automation (1993), pp.277–282, DOI: 10.1109/ROBOT.1993.291995.

27. Včelák, J., Ripka, P., Kubik, J., Platil, A. and Kašpar, P., AMR navigation systems and methods of their calibration, Sensors and Actuators A: Physical, Vol.123-124 (2005), pp. 122-128, DOI: 10.1016/j.sna.2005.02.040.
28. Sabatini, A. M., Quaternion-based extended Kalman filter for determining orientation by inertial and magnetic sensing, IEEE Transactions on Biomedical Engineering, Vol. 53, No. 7 (2006), pp.1346-1356, DOI: 10.1109/TBME.2006.875664.
29. Zhu, R. and Zhou, Z., Calibration of three-dimensional integrated sensors for improved system accuracy, Sensors and Actuators A: Physical, Vol.127, No.2 (2006), pp. 340-344, DOI: 10.1016/j.sna.2005.12.001
30. Rogers, R. M., Applied mathematics in integrated navigation systems, Second edition, AIAA Education Series (2003).
31. Ae, M., Tang, H. and Yokoi, T., Estimation of inertia properties of the body segments in Japanese athletes, Biomechanism, Vol.11 (1992), pp.23–33 (in Japanese).
32. Yamamoto, H. and Yanagida, Y., The various patterns of knee angle in the stance phase, The Society of Physical Therapy Science, Vol. 26, No. 2 (2011), pp. 269-273 (in Japanese).